Structures 79 (2025) 109449

Contents lists available at ScienceDirect

Structures

journal homepage: www.elsevier.com/locate/structures

Mitigation measure using tuned mass dampers for torsional irregularity impact on seismic response of L-shaped RC structures with soil–structure interaction

Ibrahim Oz [a,*,1], Sheheta E. Abdel Raheem [b,2], Canan Turan [a,3]

[a] Dept. of Civil Engineering, Kirsehir Ahi Evran Univ., Kırsehir 40100, Turkey
[b] Dept. of Civil Engineering, Faculty of Engineering, Assiut Univ., Assiut 71516, Egypt

ARTICLE INFO

Keywords:
Mitigation measure
TMD
Torsional irregularity
L-shaped RC structures
SSI

ABSTRACT

This study investigates the effectiveness of tuned mass damper (TMD) systems in mitigating torsional irregularities impact on seismic response of L-shaped reinforced concrete (RC) buildings, with a particular emphasis on soil–structure interaction (SSI) effects. Nonlinear time history analyses were conducted on a nine-story RC building constructed on both ZC (moderate) and ZD (soft) soil types, under three different conditions: fixed-base, SSI without control, and SSI with TMD control. The SSI effects were modeled using a substructure approach, and 15 bidirectional ground motion records were used for input excitation for each case. This paper presents a novel configuration of TMDs on building roof; the effectiveness of TMD in mitigating seismic responses of L-Shaped RC Structures subjected to a range of earthquake ground motions is assessed. This study investigates how torsional behavior is affected by soil–structure interaction (SSI) and how this behavior can be mitigated through the implementation of TMDs. The outcome results show that SSI notably amplifies torsional responses, especially in soft soils, leading to higher exceedance probabilities of the torsional irregularity index η_{bi}. The introduction of the TMD control system significantly reduced torsional irregularities impact on seismic demands, with a reduction exceeding 12 % in upper stories for ZD soils. Fragility curves further confirmed the TMD's effectiveness in reducing the probability of torsional irregularity impact exceedance. These findings highlight the necessity of incorporating SSI effects on seismic demands assessment and the effectiveness of TMD control devices for seismic mitigation as a seismic design approach for irregular RC buildings.

1. Introduction

Recent earthquakes have demonstrated the necessity for reinforced concrete (RC) buildings to retain sufficient strength under seismic loading. Irregular and asymmetric multi-story structures are highly vulnerable to earthquake damage due to lateral and torsional vibration coupling, leading to more brittle behavior of the overall structure [1,2]. Torsional irregularity or asymmetry in the building occurs due to the uneven distribution of mass and eccentricity between the center of resistance. This asymmetry will lead to lateral and torsional displacement during strong earthquake ground motions. In this context, torsional behavior has gained significance in the analysis and design of RC buildings [3]. Torsional behavior, in this regard, is defined by the Torsional Irregularity Coefficient (η_{bi}) which represents the ratio of the maximum relative story displacement in any story to the average relative displacement in the same direction, considering two orthogonal earthquake directions. According to the Turkish Building Earthquake Code [4], the building has torsional irregularity if η_{bi} exceeds 1.2

To achieve the desired seismic performance, a building should exhibit key attributes such as a regular configuration, and sufficient lateral strength, stiffness, and ductility. Therefore, the selection of the building's plan configuration at the conceptual design stage plays a crucial role in structural design against earthquake-induced ground motions. In practical applications, most buildings present some form of

* Corresponding author.
E-mail addresses: ibrahim.oz@ahievran.edu.tr (I. Oz), shehataraheem@eng.au.edu.eg (S.E. Abdel Raheem), canan.turan@ahievran.edu.tr (C. Turan).
[1] ORCID: https://orcid.org/0000-0003-3152-3675.
[2] ORCID: https://orcid.org/0000-0002-9576-2563.
[3] ORCID: https://orcid.org/0000-0003-2061-6657.

https://doi.org/10.1016/j.istruc.2025.109449
Received 12 May 2025; Received in revised form 9 June 2025; Accepted 12 June 2025
Available online 18 June 2025

irregularity, making torsional-lateral vibration coupling effects inevitable under seismic excitation [5]. Building structures with irregular planes are more susceptible to seismic forces than regular ones. The reason is that the center of mass has different positions from the center of rigidity in the irregular frame structure, and the torsional deformation of the structure caused by eccentricity is more likely to lead to structural failure. Consequently, the design and seismic performance evaluation of RC buildings affected by torsional irregularity effects is considerably more complex compared to symmetric buildings [3]. Unfortunately, eliminating torsional irregularities is not a feasible approach in civil engineering practice [3]. Therefore, preventive measures must be taken to mitigate torsional behavior. The asymmetric distribution of mass, stiffness, and strength due to plan irregularity in L-shaped buildings is a major contributor to severe damage caused by excessive floor rotations and displacements [3,6].

In addition, several studies in the literature have investigated the torsional behavior of L-shaped buildings. Ozer et al. [7] evaluated the seismic performance of lead-core rubber (LRB) and friction pendulum (FPS) base isolators under torsional irregularity, revealing that the performance of LRB isolators was more sensitive to torsional effects, that the misalignment between the superstructure's center of mass and the isolator's center of rigidity is dominant parameter that control torsional response and displacement demands. Gokdemir et al. [8] examined the impact of torsional irregularity on seismic vulnerability, showing that eccentricity between the centers of mass and rigidity significantly increases torsional moment demands, potentially leading to structural failure during earthquakes. Their findings underscore the importance of symmetric design and sufficient separation between structural components to reduce damage. Abdel Raheem et al. [9] assessed the seismic performance of multi-story L-shaped RC buildings, demonstrating that increased plan irregularity considerably amplifies torsional effects, lateral displacements, and shear demands factors that conventional design codes often underestimate. These results highlight the necessity for detailed dynamic analysis and irregularity-specific design considerations. Botis, Cerbu [10] proposed a theoretical and computational method to minimize torsional effects in irregular reinforced concrete multi-storey buildings by optimizing the alignment between centers of mass and stiffness using MATLAB and validating results through ETABS simulations. Ismail [11] introduced a novel seismic design method for Symmetric Released Column Inclination (SRCI) control that reduces structural torsion, base shear, and accelerations in asymmetric multi-storey buildings through column-end modifications and a custom damping brace system, as validated by nonlinear time history analyses. Khanal, Chaulagain [12] evaluated the seismic elastic performance of regular and L-shaped reinforced concrete buildings with varying plan irregularities and seismic incidence angles, revealing that increased irregularity and off-axis loading significantly amplified displacement, drift, and torsional responses, suggesting that current code provisions are inadequate for irregular structures. It could be concluded that the floor shape plays a considerable role in the seismic behavior of mid-rise moment resisting frame (MRF) building including a substantial increase in the lateral deflections and inter-story drifts and changing the performance level of the structures and pursued functionality. Thus, considering plan irregularity effects in the seismic design, particularly when floor shape is mostly used in vital buildings is essential. If irregularity is not considered in dynamic analysis and design, the accuracy in assessing the structural safety, facing earthquakes, could not be reliable. The conventional design procedures excluding the horizontal irregularity may not be adequate to guarantee the structural safety of irregular moment resisting building.

In recent years, there has been a growing research interest in soil–structure interaction (SSI), [13-16]. Forcellini [17] compared theoretical, experimental, and 3D numerical models of elastomeric bridge bearings, finding good agreement in initial behavior but noting the need to capture post-peak degradation due to cavitation. Kumar et al., [18] developed advanced OpenSees-based models for LDR and LR bearings to simulate their behavior under extreme seismic loads, incorporating tension effects, lead core heating, and lateral displacement-dependent buckling. Asgari et al., [19] used 3D parallel finite element simulations to investigate the seismic resilience of various pile group configurations in sloping liquefiable soils, revealing significant effects of pile number, position, and nonlinearity on lateral spreading, excess pore pressure, and foundation performance compared to existing design codes. Forcellini [20,21] proposed a simplified three-degree-of-freedom (3-DOF) model to evaluate the coupled effects of soil-structure interaction (SSI) and base isolation (BI) in low-rise buildings, demonstrating that SSI can considerably reduce or even reverse the expected seismic benefits of BI systems. Fiamingo, Massimino [22] conducted a large-scale investigation into the dynamic soil-structure interaction (DSSI) effects on historical churches in the highly seismic eastern Sicilian region, aiming to prioritize seismic retrofitting interventions by assessing the influence of soil behavior and masonry properties on the seismic response under both fixed-base and flexible-base configurations. Mina, Forcellini [23] conducted a 3D numerical study using OpenSeesPL to assess soil–structure interaction during the 1980 Irpinia–Basilicata earthquake, revealing that soil deformability notably amplifies seismic demands on low-rise RC buildings and should be integrated into seismic design codes. Massimino et al., [24] investigated the seismic performance of eco-friendly soil–rubber mixtures (SRMs), presenting findings from seismic microzonation, site response, and soil–structure interaction studies, along with results from full-scale tests and FEM simulations. Abate et al., [25] proposed an innovative large-scale seismic microzonation approach for Catania by evaluating dynamic soil–structure interaction (DSSI) through spectral acceleration maps, and further analyzed the nonlinear soil response of a school building using FEM models with different soil nonlinearity assumptions. Farhad, Aydın [26] proposed an optimization method for the placement of viscous dampers between low-rise adjacent buildings to minimize seismic pounding, explicitly considering the effects of soil–structure interaction under different sandy soil conditions. Kalfas et al. [27] analyzed how shear modulus influences elastomeric bearing behavior under axial-shear loads and proposed a nonlinear closed-form solution. Although numerous studies in the literature focus on base isolation and various TMD systems, there is limited research directly addressing the reduction of torsional irregularities in L-shaped buildings using TMDs.

The primary objective of this study is to assess the torsional irregularity impact on seismic demands of L-shaped multi-story buildings, evaluate the effectiveness of tuned mass damper systems in mitigating the torsional response of structures subjected to dynamic loading. Gutierrez Soto, Adeli [28] reviewed key developments in the design and application of various mitigation measures tuned mass dampers including: conventional, pendulum, bidirectional, and tuned liquid column dampers highlighting their effectiveness in vibration mitigation of buildings and civil structures under dynamic loads such as wind and earthquakes. Rana, Soong [29] investigated the behavior of tuned mass dampers through a detailed parametric analysis and proposed a simplified design procedure to optimize their performance in reducing structural vibrations, including an evaluation of multi-mode control using multiple dampers. Sadek et al., [30] proposed a numerical procedure for determining optimal tuned mass damper parameters that achieve equal and large modal damping in the first two vibration modes of structures, demonstrating through analyses of single degree of freedom (SDOF) and multi degree of freedom (MDOF) systems, their method significantly introduced reduced seismic responses compared to previous approaches. Konar, Ghosh [31] provided a comprehensive review of the development and application of tuned mass damper inerter (TMDI) systems over the past decade, highlighting their effectiveness in reducing seismic responses in multi-story buildings through mass amplification, while identifying key research gaps for practical implementation. Marrazzo et al., [32] investigated the seismic retrofitting of existing buildings using non-conventional tuned mass dampers with high mass ratios, demonstrating through extensive parametric analysis

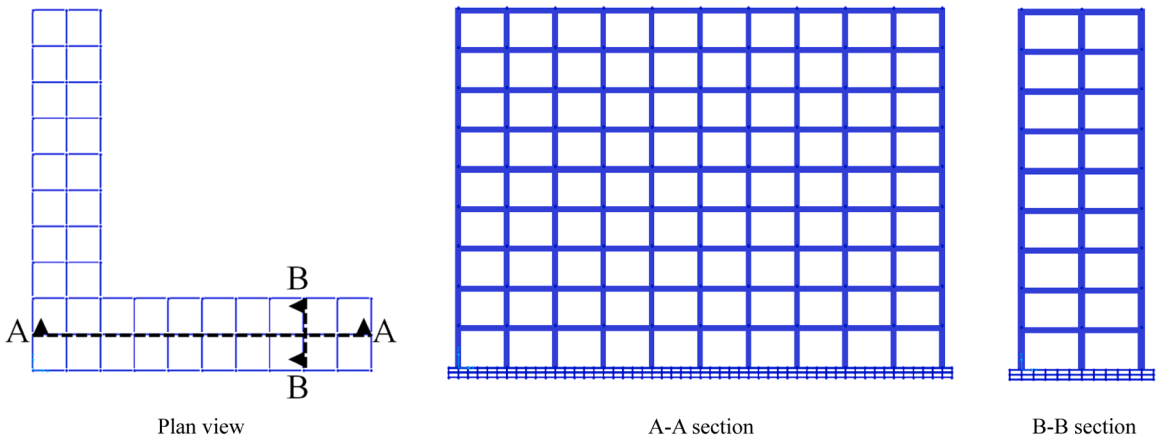

Fig. 1. Plan and wing views of the investigated L-shaped structure.

and a case study that such systems significantly reduced displacements, accelerations, and structural damage, thereby improving seismic resilience, particularly in buildings designed to outdated codes. Araz [33] studied the influence of soil-structure interaction (SSI) effect on the control performance and optimum parameters of tuned mass damper (TMD), the effect of structure stiffness and soil stiffness and the aspect ratio of the structure on the optimum design of TMD, the seismic performance of structures and highlight that the effectiveness of TMD will vary significantly depending on the characteristics of the ground motion due to SSI effects. Fatollahpour et al., [34] investigated the impact of structure–soil–structure interaction (SSSI) on the seismic performance of two adjacent 20-story buildings equipped with optimized tuned mass dampers (TMDs), finding that while SSSI significantly amplifies seismic responses, the use of PSO-optimized TMDs effectively reduces both maximum and RMS story drifts even under these interaction effects. While most TMD studies in the literature focus on plan optimization or device design, this study uniquely addresses the overlooked relationship between TMDs and torsional irregularity.

This study investigates the prevention of torsional behavior in irregular reinforced concrete buildings through the design and implementation of Tuned Mass Damper (TMD) systems. In line with this objective, nonlinear time history analyses were conducted on an L-shaped reinforced concrete building situated on ZC and ZD type soils as defined by seismic design codes. The analyses were performed under three conditions: fixed base without control, soil-structure interaction (SSI) without control, and SSI with TMD control, under 15 bidirectional ground motion records for each case, with a total of 30 acceleration records. SSI effects were modeled using the substructure method. In this method, ground motion records were selected to reflect the properties of the respective soil types 15 for ZC-type soil and 15 for ZD-type soil. Analysis results indicated that SSI effects had a negative influence on torsional behavior, while this negative impact was effectively mitigated by simple TMD systems installed on the roof of the structure.

2. Materials and methods

2.1. Design of the structures

Since the primary aim of this study was to control torsional irregularity, the selected building model was deliberately designed to exhibit torsional behavior. Accordingly, an L-shaped plan layout, which is frequently used in literature for studies on torsional irregularity, was adopted. The analyzed structure is a nine-story reinforced concrete frame building. The height of the first story was taken as 3.5 m, while the remaining stories were each 3.3 m tall, resulting in a total building height of 29.9 m. The columns were designed with cross-sectional dimensions of 60 × 60 cm, and the beams were modeled as 25 × 50 cm members. End-length offsets were defined at beam-column joints based on the member dimensions, and a rigid zone factor of 0.5 was applied. The plan view of the investigated L-shaped building, along with the long and short sections of the L-shape, is shown in Fig. 1.

In accordance with TBEC-2018, reduced effective moment of inertia values (*Ieff*) were used for both design and evaluation stages. Specifically, the effective stiffness was defined as 0.35I for beams and 0.7I for columns, following the guidelines of the TBEC-2018. Given that the building represents a new construction, the transverse reinforcement spacing specified in the current code was adopted, with stirrup spacing set to 10 cm. No section reduction was made in vertical load-bearing elements due to story height. The bay spacing was uniformly set to 5 m throughout the building. Each L-shaped wing consisted of 8 spans, while the central joint zone of the L form included 2 spans. The total length of the building arms was 50 m, of which 10 m belonged to the central intersection region. The structural behavior factor (R) was taken as 8, reflecting the fact that the system consists solely of moment-resisting frames. A uniform slab thickness of 12 cm was considered for all stories. Live loads were taken as 200 kg/m^2 (0.2 t/m^2), and dead loads as 325 kg/m^2 (0.325 t/m^2). The slabs were not explicitly modeled; instead, the loads were applied directly onto the beams. Both design and evaluation stages considered second-order (P-Δ) effects. To account for infill wall weights, a uniform line load of 0.19 t/m was assigned to the relevant beams.

The three-dimensional structural models were developed using SAP2000 version 23.3.1 [35], a widely used platform for dynamic structural analysis. To simulate nonlinear behavior, fiber-based lumped plastic hinge elements were utilized, where the nonlinear response arises directly from material properties. Each hinge was modeled using a fiber section approach, and stiffness degradation was based on the actual material response. One hinge per end was sufficient to capture biaxial bending behavior, following the methodology of Carvalho et al. [36]. The plastic hinge length was assumed as 0.5 times the section height. Concrete compressive strength was assumed to be 30 MPa, and the yield strength for both longitudinal and transverse reinforcements was 420 MPa. Post-yield strain hardening effects were also considered in the analysis.

Time-history analyses were performed using the Newmark-beta method [37]. To ensure unconditional numerical stability, the parameters gamma (γ) and beta (β) were set to 0.5 and 0.25, respectively. Rayleigh damping was used for the damping model, with a damping ratio of 5 %. The mass and stiffness proportional damping coefficients were determined based on selected mode periods to implement viscous damping. The number of modes included in the analysis was chosen to ensure cumulative mass participation exceeding 95 %, which corresponded to the first 24 modes in this study.

Table 1
Considered soil properties.

Property	ZC	ZD
Mass density ρ (kN/m^3)	16	20
Poisson's ratio	0.30	0.25
V_{s30} (m/s)	400	200

2.2. Soil-Structure modelling approach

The substructure method was adopted in this study to incorporate the effects of soil–structure interaction (SSI). A crucial step in applying this method involves calculating the foundation impedance functions, as these significantly influence the dynamic characteristics of a structure, including its natural period [38-41]. These influences are often referred to as inertial interaction effects [42]. The substructure method is typically categorized into lumped parameter models and cone models. In this research, a lumped parameter approach was employed, where foundation stiffness and damping were simulated using discrete spring-dashpot systems. It is important to note that most lumped models are based on simplified conditions, such as shallow foundations resting on homogenous elastic half-spaces [42].

The foundation–soil system was modeled using linear elastic springs and dashpots connected to the superstructure via foundation elements, as suggested by NIST [42]. The corresponding stiffness and damping values were calculated using established formulations provided by NIST [42], which are widely referenced in the literature (e.g., [43,13,44-46]). The soil shear modulus was determined using Eq. (1), where Vs is the shear wave velocity, G is the shear modulus, and ρ is the soil density. Mechanical parameters such as density and Poisson's ratio are listed in Table 1.

$$Vs = \sqrt{\frac{G}{\rho}} \tag{1}$$

To evaluate the spring and dashpot parameters, key inputs included average shear-wave velocity, Poisson's ratio, foundation dimensions (length, width, depth), and the structural natural period. Soil classes ZC and ZD were assumed to have shear wave velocities of 400 m/s and 200 m/s, respectively, as per recommendations by the (TBEC-2018)

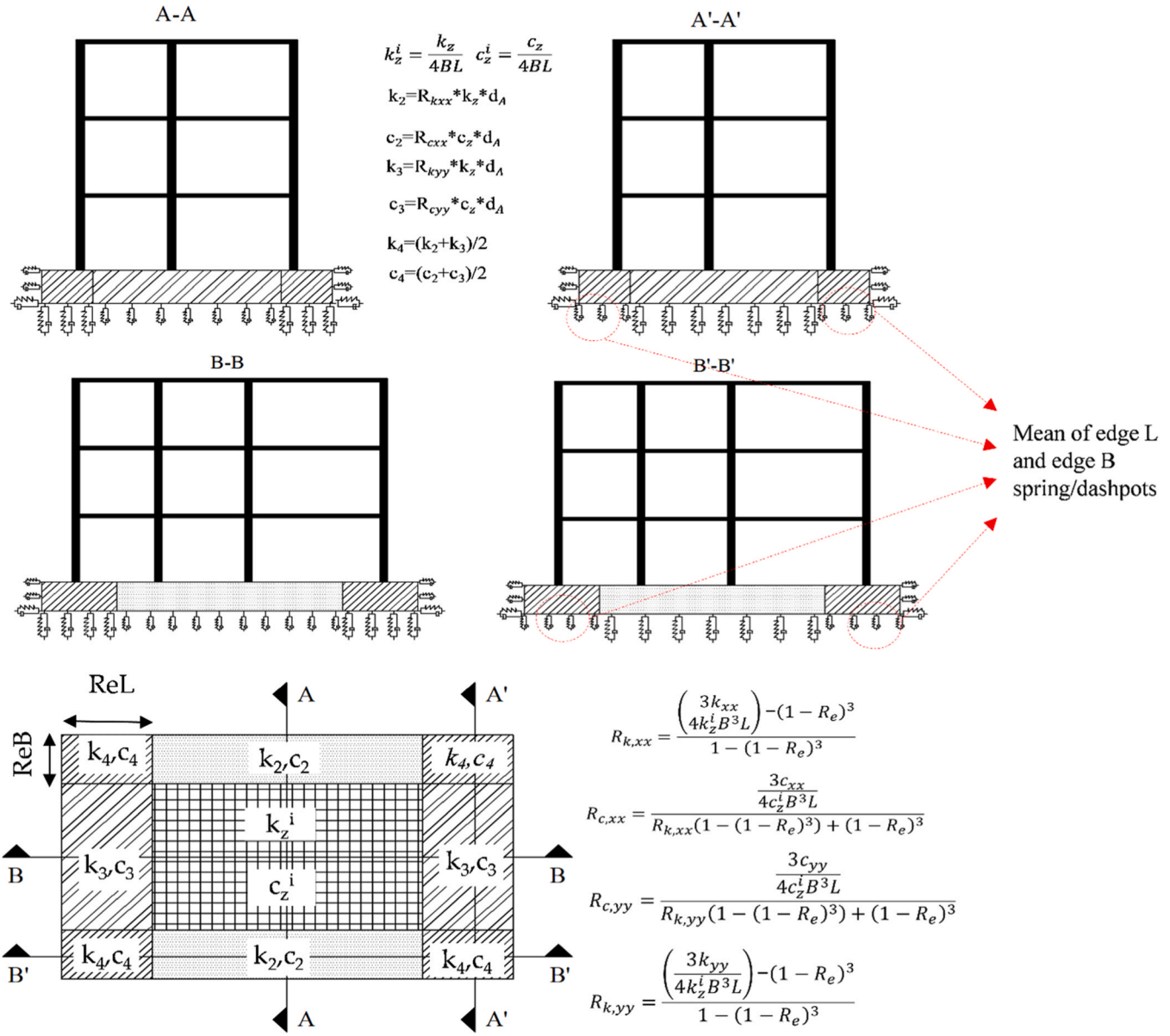

Fig. 2. SSI modeling: stiffness and damping expressions for raft foundation systems.

Table 2
The formulas used for calculating soil springs [33].

Radiation Damping Ratios for Embedded Footings	Elastic Solutions for Static Stiffness of Rigid Footings at the Ground Surface
$\beta_z = \left[\frac{4[\psi(L/B)+(D/B)(1+L/B)]}{(K_{z,emb}/GB)}\right]\left[\frac{a_0}{2\alpha_z}\right]$	$K_{z,\,sur} = \frac{GB}{1-\nu}\left[3.1\left(\frac{L}{B}\right)^{0.75}+1.6\right]$
$\beta_y = \left[\frac{4[L/B+(D/B)(1+\psi L/B)]}{(K_{y,emb}/GB)}\right]\left[\frac{a_0}{2\alpha_y}\right]$	$K_{y,\,sur} = \frac{GB}{2-\nu}\left[6.8\left(\frac{L}{B}\right)^{0.65}+0.8\left(\frac{L}{B}\right)+1.6\right]$
$\beta_x = \left[\frac{4[L/B+(D/B)(\psi+L/B)]}{(K_{x,emb}/GB)}\right]\left[\frac{a_0}{2\alpha_x}\right]$	$K_{x,\,sur} = \frac{GB}{2-\nu}\left[6.8\left(\frac{L}{B}\right)^{0.65}+2.4\right]$
$\beta_{zz} = \left[\frac{(4/3)\left[3(L/B)(D/B)+\psi(L/B)^3(D/B)+3(L/B)^2(D/B)+\psi(D/B)+(L/B)^3+(L/B)\right]a_0^2}{\left(\frac{K_{zz,emb}}{GB^3}\right)\left[\left(\frac{1.4}{1+3(L/B-1)^{0.7}}\right)+a_0^2\right]}\right]\left[\frac{a_0}{2\alpha_{zz}}\right]$	$K_{zz,sur} = GB^3\left[4.25\left(\frac{L}{B}\right)^{2.45}+4.06\right]$
$\beta_{yy} = \left[\frac{(4/3)\left[\left(\frac{L}{B}\right)^3\left(\frac{D}{B}\right)+\psi\left(\frac{D}{B}\right)^3\left(\frac{L}{B}\right)+\left(\frac{D}{B}\right)^3+3\left(\frac{D}{B}\right)\left(\frac{L}{B}\right)^2+\psi\left(\frac{L}{B}\right)^3\right]a_0^2}{\left(\frac{K_{yy,emb}}{GB^3}\right)\left[\left(\frac{1.8}{1+1.75(L/B-1)}\right)+a_0^2\right]}+\frac{\left(\frac{4}{3}\right)\left(\frac{L}{B}+\psi\right)\left(\frac{D}{B}\right)^3}{\left(\frac{K_{yy,emb}}{GB^3}\right)}\right]\left[\frac{a_0}{2\alpha_{yy}}\right]$	$K_{yy,sur} = \frac{GB^3}{1-\nu}\left[3.73\left(\frac{L}{B}\right)^{2.4}+0.27\right]$
$\beta_{xx} = \left[\frac{(4/3)\left[\left(\frac{D}{B}\right)+\left(\frac{D}{B}\right)^3+\psi\left(\frac{L}{B}\right)\left(\frac{D}{B}\right)^3+3\left(\frac{D}{B}\right)\left(\frac{L}{B}\right)+\psi\left(\frac{L}{B}\right)\right]a_0^2}{\left(\frac{K_{xx,emb}}{GB^3}\right)\left[\left(\frac{1.8}{1+1.75(L/B-1)}\right)+a_0^2\right]}+\frac{\left(\frac{4}{3}\right)\left(\psi\frac{L}{B}+1\right)\left(\frac{D}{B}\right)^3}{\left(\frac{K_{xx,emb}}{GB^3}\right)}\right]\left[\frac{a_0}{2\alpha_{xx}}\right]$	$K_{xx,\,sur} = \frac{GB^3}{1-\nu}\left[3.2\left(\frac{L}{B}\right)+0.8\right]$

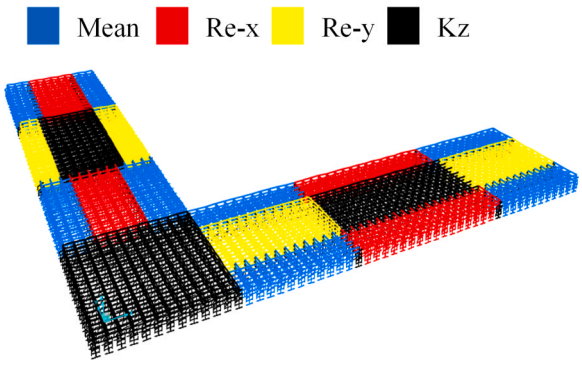

Fig. 3. Spring groups and their layout used in the L-shaped building.

[47] and NEHRP [48]. To account for the reduction in shear modulus at large strain levels, the values were adjusted in accordance with the G/G_{max} degradation approach recommended in Section 19 of ASCE [49]. The average shear modulus and corresponding shear wave velocity (Vs) were determined based on the strain levels and reference values provided in Table 19.2–1 of the standard.

Initial impedance functions were calculated assuming surface foundations (zero embedment) and were then adjusted using dynamic stiffness modification factors to account for embedment depth. The stiffness modifiers were determined based on the structure's fundamental vibration periods in the X and Y directions (Tx and Ty), as these values directly influence the dynamic characteristics considered in the SSI analysis. Likewise, radiation damping ratios were derived according to soil and structural characteristics. Modified spring and dashpot properties were then used to obtain vertical stiffness and damping coefficients k_z^i and c_z^i, respectively. As vertical soil response is nonlinear, stiffness values for central foundation areas were increased, while damping values were reduced toward the edges. An edge ratio of 0.3 was

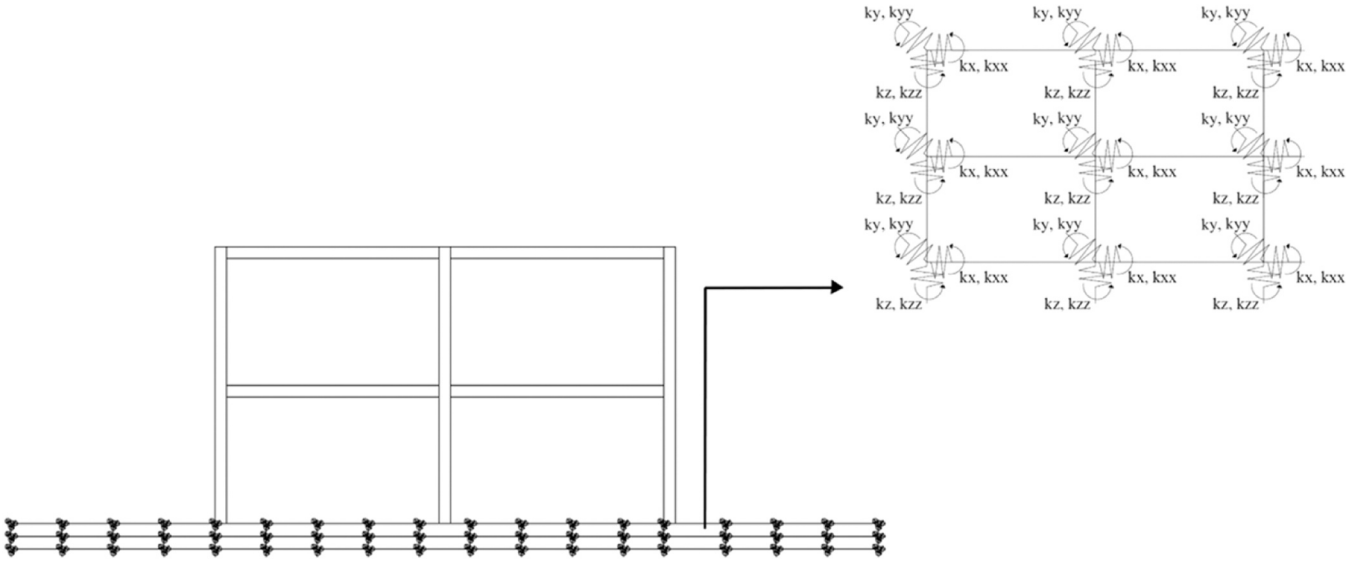

Fig. 4. Schematic illustration of connection of soil link-foundation and superstructure elements.

Table 3
Period elongations by SSI effects.

Model	Mode 1 (sec)	Mode 2 (sec)	Mode 3 (sec)
FB	1.671	1.592	1.515
SSI-ZC	1.827	1.711	1.629
SSI-ZD	2.005	1.973	1.917

Table 4
TMD properties.

Model	ZC	ZD
k(x and y) (kN/m)	232.058	198.659
c (x and y) (kNs/m)	45.527	42.124
mass (ton/m^2)	0.202	0.202

adopted, consistent with typical values ranging between 0.3 and 0.5. Foundation elements were modeled based on previous works [42,50,44,45], using elastic frame members connected to the base of ground-story columns. These members were capable of resisting combined vertical, horizontal, and moment loads without the use of hinges. Fig. 2 illustrates the spring and dashpot configurations at the foundation–soil interface. Notably, spring elements only respond to forces aligned with their axis [42]; perpendicular loads do not influence their behavior. Consequently, stiffness and damping properties were directionally assigned as uniaxial link elements to accurately simulate SSI across differential surface areas. The validation of the SSI model used in this study through the linear direct method was also carried out in the study by [44]. In the method under consideration, the surface stiffness values are to be multiplied by the embedment effects, and the radiation damping for embedded footings is given by the formulas presented in Table 2.

The Fig. 3 provides a schematic of how these foundation links were integrated with the superstructure. In this study, the foundation modeled as frame elements with zero mass and discretized at 1-meter intervals in both directions. The foundation elements were defined to allow internal rotations and flexural deformations. To maintain consistency with the fixed-base (FB) model, the FB structure was also modeled with foundation elements, and the base of these elements was defined as fixed. The spring representations assigned to the foundation elements are illustrated in Fig. 4.

The analysis results revealed that the inclusion of SSI consistently led to an elongation of the natural vibration periods when compared to the fixed-base models across all cases. This elongation typically results in a reduction of spectral acceleration, thereby decreasing seismic demands. However, the extent of this reduction varies and depends on factors such as foundation stiffness and soil conditions. Consequently, incorporating SSI into seismic design and evaluation is essential. Table 3 summarizes the increase in natural periods due to SSI effects observed in the analyzed structures.

Table 5
Frequency ratios of the TMD systems relative to the structural models.

	Frequency ratio		
Model	Mode 1 (sec)	Mode 2 (sec)	Mode 3 (sec)
SSI-ZC	89.10 %	83.45 %	79.45 %
SSI-ZD	90.38 %	88.94 %	86.42 %

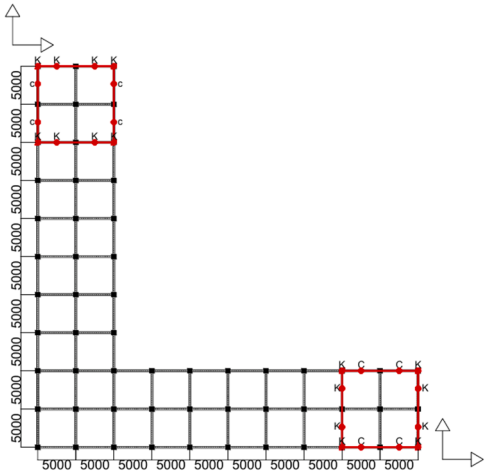

Fig. 6. The plan layout and movement directions of the TMDs.

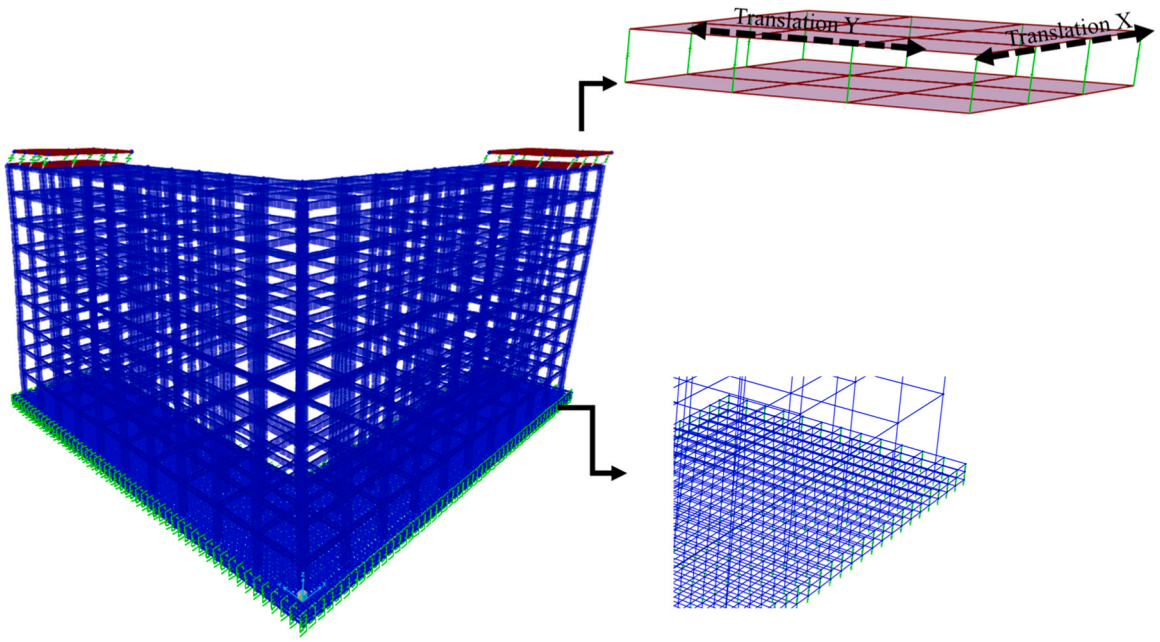

Fig. 5. Three-dimensional finite element model of the L-shaped reinforced concrete structure, illustrating the implementation of SSI through linear springs at the foundation level and the integration of tuned TMDs at the roof level to mitigate seismic responses.

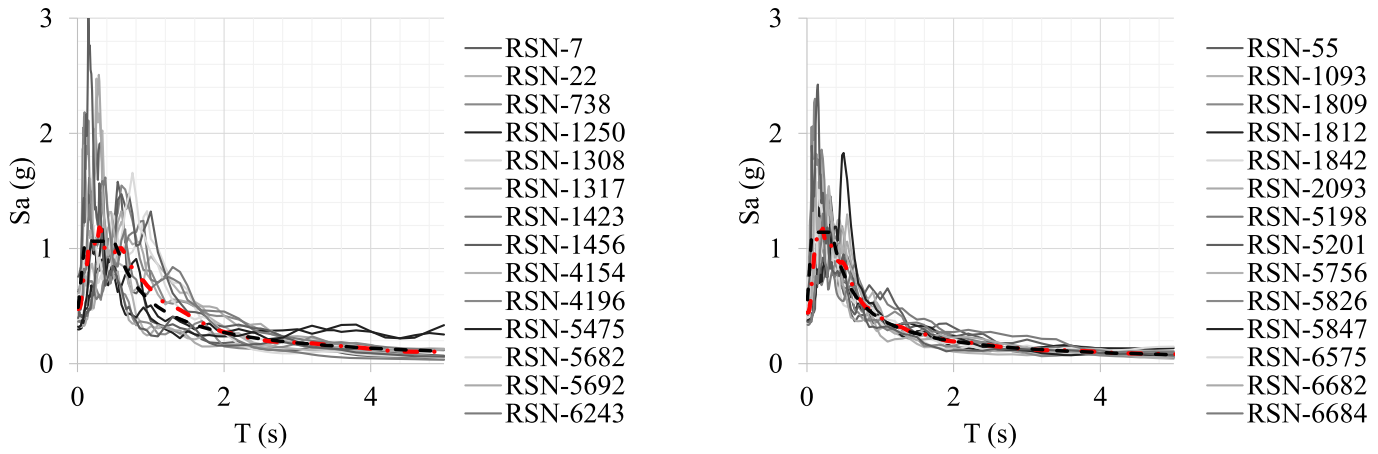

Fig. 7. Acceleration response spectra of the selected ground motions ZD (left), ZC (right).

Table 6
Statistical values for ZD cases.

Model	Story 1	Story 2	Story 3	Story 4	Story 5	Story 6	Story 7	Story 8	Story 9
FB-Mean	1.097	1.093	1.083	1.066	1.052	1.045	1.057	1.073	1.081
FB-Std	0.131	0.122	0.123	0.124	0.120	0.113	0.106	0.109	0.110
SSI-Mean	1.017	1.084	1.131	1.149	1.151	1.163	1.174	1.173	1.173
SSI-Std	0.079	0.085	0.089	0.096	0.108	0.111	0.108	0.106	0.096
TMD-Mean	1.054	1.059	1.062	1.055	1.047	1.038	1.032	1.028	1.022
TMD-Std	0.046	0.048	0.048	0.044	0.035	0.029	0.026	0.018	0.014

Table 7
Statistical values for ZC cases.

Model	Story 1	Story 2	Story 3	Story 4	Story 5	Story 6	Story 7	Story 8	Story 9
FB-Mean	1.088	1.089	1.088	1.086	1.083	1.075	1.067	1.063	1.067
FB-Std	0.087	0.092	0.097	0.109	0.126	0.144	0.153	0.153	0.148
SSI-Mean	1.052	1.114	1.132	1.129	1.124	1.121	1.109	1.105	1.111
SSI-Std	0.093	0.101	0.104	0.104	0.115	0.132	0.147	0.149	0.138
TMD-Mean	1.048	1.051	1.051	1.049	1.046	1.043	1.038	1.035	1.030
TMD-Std	0.024	0.024	0.029	0.029	0.026	0.022	0.015	0.012	0.008

2.3. Tuned mass damper models

In this study, conventional tuned mass damper (TMD) systems were utilized. For the TMD to effectively reduce structural vibrations, mass, stiffness, and damping values must be selected appropriately. The mathematical formulations corresponding to these systems are presented between Eq. (2) and Eq. (5) [51]. In these equations, μ denotes the mass ratio between the TMD mass (m_d) and the structural mass (m_s), ks represents the stiffness of the structure, while k_d and cd correspond to the stiffness and damping coefficient of the damper, respectively. ξ_d is the damping ratio of the TMD, and γ refers to the frequency ratio between the TMD (ω_d) and the primary structure (ω_s).

$$\mu = \frac{m_d}{m_s} \tag{2}$$

$$\omega_{d^2} = \frac{k_d}{m_d} \tag{3}$$

$$\xi_d = \frac{c_d}{2\omega_d m_d} \tag{4}$$

$$\gamma = \frac{\omega_d}{\omega_s} \tag{5}$$

Within the scope of this study, the TMD damping ratio was considered as 15 %, and the TMD mass ratio was taken as 1.5 %. The numerical model included 16 springs representing stiffness (k) characteristics and 8 dashpots representing damping (c) behavior of TMD. Since this study models the torsional behavior of an L-shaped reinforced concrete building under bi-directional time-history earthquake analyses, the TMD system was also modeled in three dimensions. Each TMD was configured to allow displacement in both orthogonal directions (X and Y), thereby enabling effective energy dissipation along both axes. The lower plate of the TMD was assigned the same boundary conditions as the building to ensure consistent interaction with the structure, while the upper mass provided the damping effect through its relative motion. The calculated stiffness and damping coefficients of the TMDs are presented in Table 4. The implementation of the TMD system on L shape structure is illustrated in Fig. 5.

Mathematical models of the L-shaped frame structure, both with and without TMDs, are developed through theoretical analysis, and corresponding computational programs are implemented. Subsequently, the time history responses under bi-directional seismic excitation are evaluated, and the effects are examined by assessing torsional irregularities derived from displacement responses.

The TMD systems were used with identical properties in both principal directions (x and y), and the frequency ratios between the structures and the TMD systems for the first three modes are presented in Table 5. The movement directions and plan views of the TMDs are shown in Fig. 6. All dimensions in the figure are in millimeters.

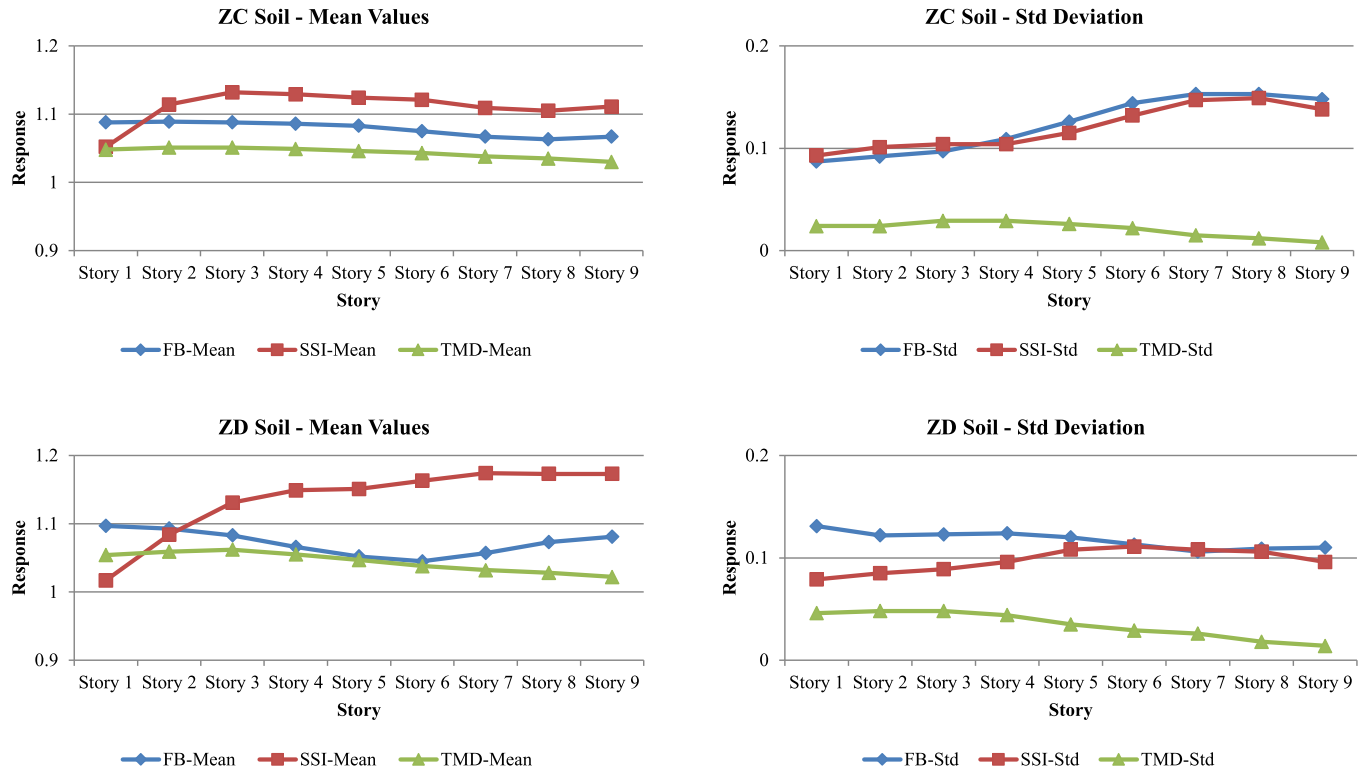

Fig. 8. Means and standard deviations of maximum torsional responses.

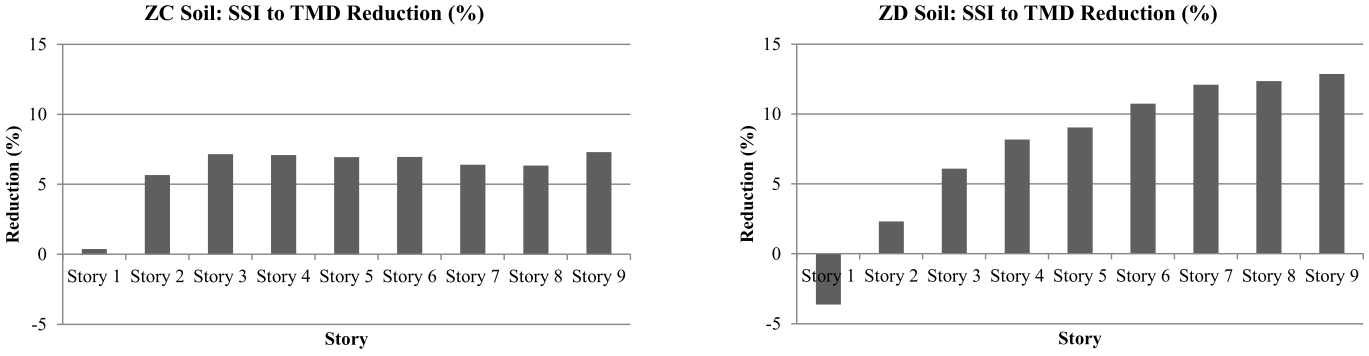

Fig. 9. Reduction ratios of TMD system.

3. Analyze results and discussion

In this study, 15 ground motion records for each ZC and ZD soil type were obtained from the PEER [52] Strong Ground Motion Database [53–55]. During the selection process, particular attention was paid to ensuring that the shear wave velocity (V_{s30}) of the station for ZC-type soils fell within the range of 380–420 m/s. As previously noted, a representative Vs value of 400 m/s was considered for ZC soils. For ZD-type soils, the V_{s30} range was defined as 180–220 m/s. Additionally, for both soil types, ground motion records with a moment magnitude (Mw) greater than 6.5 and epicentral distances ranging between 70 and 130 km were selected. The response spectra of the selected ground motion records along with their mean spectrum, and design based (DBE) spectrum [56] are presented in Fig. 7, where the DBE spectrum corresponds to a return period of 475 years.

After determining the minimum (Δ_{imin}) and maximum (Δ_{imax}) displacements per story as specified in the code from the displacements obtained from the nonlinear dynamic time history analyses, the averages ($\Delta_{iaverage}$) of these displacements were calculated, and the torsional behavior coefficient was computed separately for each story. These expressions are given by $\Delta_{iaverage}$ in Eq. (6), and the story torsional behavior coefficient ηbi is calculated using Eq. (7).

$$\Delta iaverage = \frac{\Delta imax - \Delta imin}{2} \tag{6}$$

$$\eta bi = \frac{\Delta imax}{\Delta iaverage} \tag{7}$$

The average of the maximum torsional irregularities at each story, obtained from the analysis of 15 ZC and 15 ZD ground motion records, along with their corresponding standard deviation values, are presented in Table 6 and Table 7.

The Fig. 8 illustrates the increase in mean torsional response demands and their standard deviations due to soil-structure interaction (SSI) for both ZD and ZC soil types compared to that of fixed-base condition. The results indicate that SSI significantly amplifies torsional responses, particularly in soft soil conditions. In ZD soil, the mean torsional demand increases by over 10 % in the upper stories, with a peak at Story 6. For ZC soil, the amplification remains more moderate,

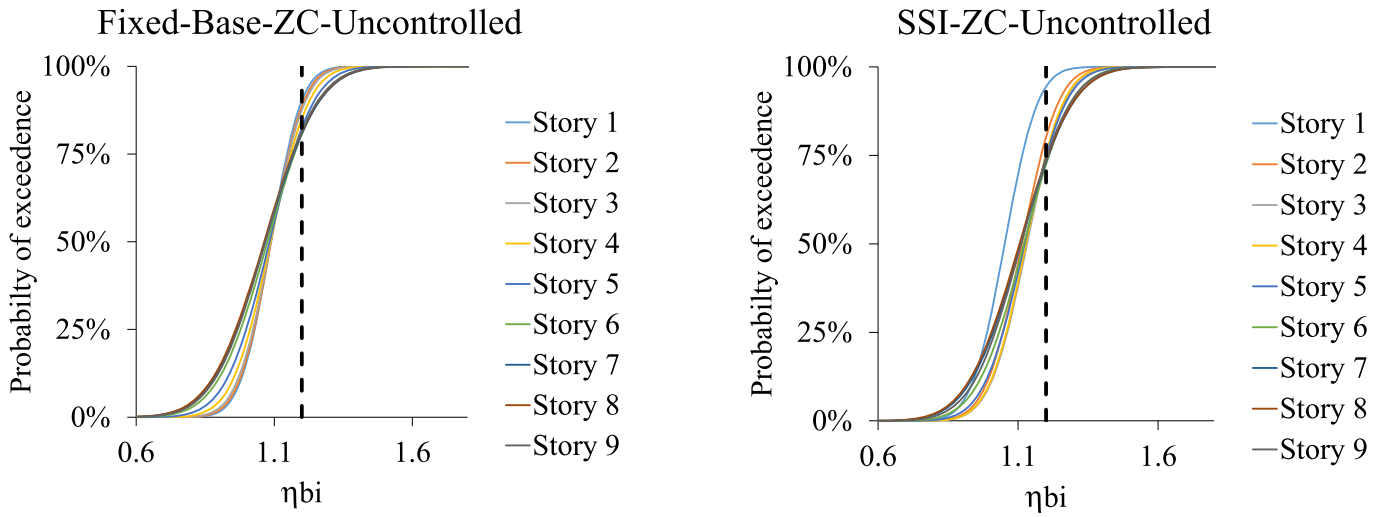

Fig. 10. Fragility curves for torsional irregularity on ZC soils (FB vs SSI).

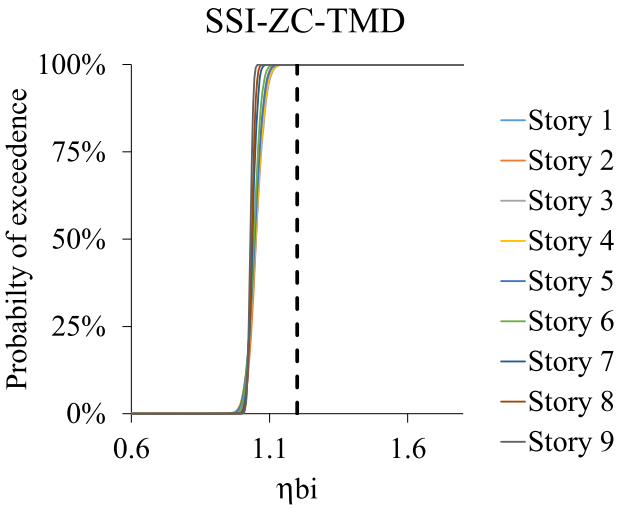

Fig. 11. Fragility curves for torsional irregularity on ZC soils (TMD).

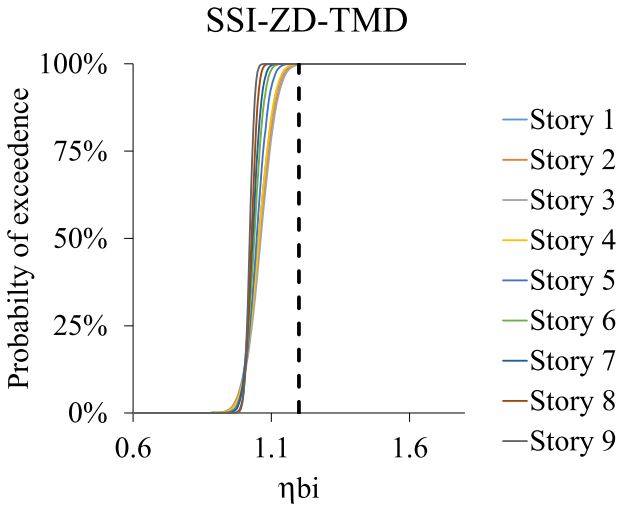

Fig. 13. Fragility curves for torsional irregularity on ZD soils (TMD).

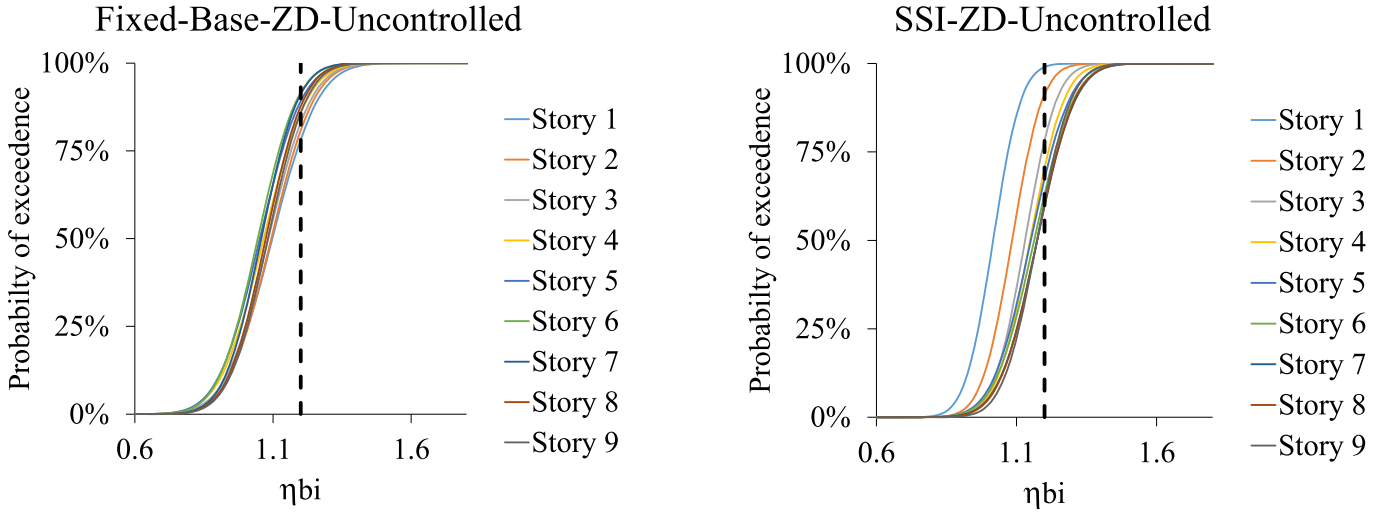

Fig. 12. Fragility curves for torsional irregularity on ZD soils (FB vs SSI).

averaging around 4 % in the upper levels. These findings confirm that SSI effects that lead to increased torsional irregularities, especially in flexible soil profiles, and should be explicitly considered in seismic design.

The Fig. 9 illustrates the percentage reduction in seismic response achieved by TMD systems relative to SSI models for both ZD and ZC soil types. The reduction of TMD system was calculated using Eq. (8).

$$\text{Reduction}(\%) = \left(\frac{SSImean - TMDmean}{SSImean}\right)x100 \quad (8)$$

In ZD soils, TMDs significantly reduce responses particularly in upper stories with reductions exceeding 12 %, highlighting their effectiveness under pronounced SSI effects. In ZC soils, where SSI-induced amplifications are less severe, the reduction remains consistent, ranging from 2 % to 8 %. These findings confirm the efficacy of TMD systems in mitigating seismic demands, particularly in flexible soil conditions.

The fragility curves presented in Figs. 9–12 are developed using a lognormal cumulative distribution function (CDF) to estimate the probability of exceeding specific damage states, with the torsional behavior coefficient (η_{bi}) used as the engineering demand parameter (EDP) [57,58]. The fragility function is formulated based on Eq. (9).

$$P(D > s|IM) = \Phi\frac{\ln(IM) - \ln(\mu)}{\sigma} \quad (9)$$

In this context: P represents the probability of structural damage (D) exceeding a given damage state; Φ denotes the standard normal cumulative distribution function; IM (η_{bi}) is the selected intensity measure value; σ is the standard deviation of the natural logarithm of the seismic intensity measure; μ is the mean of the natural logarithm of the seismic intensity measure. The mean and standard deviation values used for constructing the fragility curves for soil type ZD are presented in Table 5, while those for soil type ZC are given in Table 6.

The Fig. 10 and Fig. 11 present the probability of exceedance for the torsional irregularity index η_{bi} across nine stories under different modeling conditions for ZC soil. In the fixed-base model, several stories exhibit a moderate probability of exceeding the critical threshold of $\eta_{bi} = 1.2$, indicating inherent torsional irregularity even without soil-structure interaction (SSI). When SSI is considered, the exceedance curves shift rightward, reflecting an increase in the likelihood of torsional irregularity impact, particularly in lower stories. This demonstrates that SSI, even in relatively stiff soil conditions, negatively impacts the torsional response of the structure. However, the implementation of a tuned mass damper (TMD) under SSI conditions leads to a significant improvement: the exceedance curves become steeper and are concentrated just below the η_{bi} threshold. This confirms that TMD systems are highly effective in suppressing torsional irregularities and enhancing structural performance under seismic excitation.

The Fig. 12 and Fig. 13 demonstrate that torsional irregularities are more pronounced in ZD soil conditions for L shaped structure, particularly under SSI. Compared to ZC, the SSI-ZD model exhibits a broader and more right-shifted exceedance distribution, highlighting the amplifying effect of soft soils on torsional demands. The application of TMD systems effectively suppresses these irregularities in both cases; however, the mitigation is especially critical in ZD soil, where SSI-induced torsional amplification is more severe. These results confirm the importance of incorporating TMDs in flexible soil environments to maintain torsional stability.

4. Conclusions

This study evaluated the torsional response of L-shaped reinforced concrete structures under seismic loading, with a particular focus on the effects of soil-structure interaction (SSI) and the efficiency of tuned mass damper (TMD) as mitigation measure system. Analyses were conducted for two different site conditions ZC (stiff soil) and ZD (soft soil) based on fixed-base modeling approach, SSI-uncontrolled, and SSI-TMD structural models.

The findings demonstrated that SSI considerably amplifies torsional irregularities in L-shaped buildings, especially under soft soil conditions. The fundamental period of the structure increased from 1.671 s in the fixed-base model to 1.827 s for ZC soil and 2.005 s for ZD soil, indicating an elongation of approximately 9.3 % and 19.8 %, respectively. This elongation reflects a softening of the structural system, which not only increases overall seismic demands but also contributes to the amplification of torsional effects. For example, in ZD soil conditions, the torsional irregularity index η_{bi} across upper stories showed consistent increases under SSI effects, with values such as 1.163 at Story 6 compared to 1.045 in the fixed-base case,

Fragility curve analyses further emphasized the benefits of TMD implementation. In both ZC and ZD soils, the SSI condition increased the probability of exceeding the torsional irregularity index threshold, especially in lower and middle stories. However, with TMDs, the fragility curves shifted leftward and became steeper, indicating a notable reduction in exceedance probability and an improvement in seismic performance. These results underline the importance of considering TMDs as a viable control strategy in structures affected by torsional irregularities. The implementation of TMD systems proved to be highly effective in mitigating torsional response demands in both soil types. In ZD soils, the η_{bi} index at Story 6 was reduced from 1.163 (SSI) to 1.038 (TMD), corresponding to a 10.7 % decrease. In the upper stories, TMDs achieved reductions exceeding 12 % for ZD soil. For ZC soil, where SSI effects were less severe, the reduction ratios ranged from 2 % to 8 %, depending on the story level. These results highlight the effectiveness of TMDs in restoring torsional stability, particularly in the presence of pronounced SSI effects.

Overall, the study confirms that SSI should not be neglected in the seismic design of torsionally irregular L-shaped structures, particularly when constructed on soft soils. TMD systems provide a practical and efficient solution to mitigate torsional irregularities and enhance seismic resilience. Although this study focused on a simple TMD configuration, future research is encouraged to explore alternative damper layouts, optimized parameter combinations, and comparative studies with other seismic mitigation techniques in terms of performance and cost-effectiveness.

CRediT authorship contribution statement

Sheheta E. Abdel Raheem: Writing – review & editing, Writing – original draft, Validation, Supervision, Methodology, Investigation, Conceptualization. **Ibrahim Oz:** Software, Formal analysis, Investigation, Conceptualization, Methodology, Writing – original draft, Validation, Writing – review & editing. **Canan Turan:** Writing – review & editing, Writing – original draft, Visualization.

Declaration of Competing Interest

The authors declare that they have no known competing financial interests or personal relationships that could have appeared to influence the work reported in this paper.

References

[1] Chaker K, Sbartai B, Abdel Raheem SE. Comparative study between active AMD and ABS devices by using μ-Synthesis robust control. Appl Sci 2024;14(22):10481. https://doi.org/10.3390/app142210481.
[2] Angelis F, Cancellara D. Dynamic analysis and vulnerability reduction of asymmetric structures: fixed base vs base isolated system. Compos Struct 2019;219: 203–20. https://doi.org/10.1016/j.compstruct.2019.03.059.
[3] Abdel Raheem SE, Ahmed MM, Ahmed MM, Abdel-shafy AG. Evaluation of plan configuration irregularity effects on seismic response demands of L-shaped MRF buildings. Bull Earthq Eng 2018;16:3845–69.
[4] Ministry of Environment and Urbanization. 2018. Turkey building earthquake code. [In Turkish.] Ankara, Turkey: Earthquake Code Preparation Committee.

[5] Sucuoğlu H, Kaatsız K. Torsional ductility spectrum for predicting ductility distribution in simple asymmetric-plan structures. Earthq Eng Struct Dyn 2021;50(2):538–59.
[6] You J, Yang Y, Fan Y, Zhang X. Seismic response study of L-Shaped frame structure with magnetorheological dampers. Appl Sci 2022;12(12):5976. https://doi.org/10.3390/app12125976.
[7] Ozer E, Inel M, Cayci BT. Seismic behavior of LRB and FPS type isolators considering torsional effects. In Structures, 37. Elsevier; 2022. p. 267–83.
[8] Gokdemir H, Ozbasaran H, Dogan M, Unluoglu E, Albayrak U. Effects of torsional irregularity to structures during earthquakes. Eng Fail Anal 2013;35:713–7. https://doi.org/10.1016/j.engfailanal.2013.06.028.
[9] Abdel Raheem SE, Ahmed Momen MM, Ahmed Mohamed M, Abdel Shafy Aly GA. Seismic performance of L-shaped multi-storey buildings with moment-resisting frames. Proc Inst Civ Eng Struct Build 2018;171(5):395–408. https://doi.org/10.1680/jstbu.16.00122.
[10] Botis MF, Cerbu C. A method for reducing of the overall torsion for reinforced concrete multi-storey irregular structures. Appl Sci 2020;10(16):5555.
[11] Ismail M. New approach to seismic-resistant design and structural torsion mitigation. Eng Struct 2020;207:110092.
[12] Khanal B, Chaulagain H. Seismic elastic performance of L-shaped building frames through plan irregularities (October). In Structures, 27. Elsevier; 2020. p. 22–36 (October).
[13] Anand V, Kumar SS. Seismic soil-structure interaction: a state-of-the-art review. Vol. 16 of Structures. Amsterdam, Netherlands: Elsevier; 2018. p. 317–26.
[14] Lou M, Wang H, Chen X, Zhai Y. Structure–soil–structure interaction: literature review. Soil Dyn Earthq Eng 2011;31(12):1724–31. https://doi.org/10.1016/j.soildyn.2011.07.008.
[15] Najar IA, Ahmadi R, Amuda AG, Mourad R, Bendary NE, Ismail I, Tang S. Advancing soil-structure interaction (SSI): a comprehensive review of current practices, challenges, and future directions. J Infrastruct Preserv Resil 2025;6(1):5. https://doi.org/10.1186/s43065-025-00118-2.
[16] Islam MR, Turja SD, Van Nguyen D, Forcellini D, Kim D. Seismic soil-structure interaction in nuclear power plants: an extensive review. Results Eng 2024:102694. https://doi.org/10.1016/j.rineng.2024.102694.
[17] Forcellini D. 3D numerical simulations of elastomeric bearings for bridges. Innov Infrastruct Solut 2016;1:1–9. https://doi.org/10.1007/s41062-016-0045-4.
[18] Kumar M, Whittaker AS, Constantinou MC. An advanced numerical model of elastomeric seismic isolation bearings. Earthq Eng Struct Dyn 2014;43(13):1955–74. https://doi.org/10.1002/eqe.2431.
[19] Asgari A, Ranjbar F, Bagheri M. Seismic resilience of pile groups to lateral spreading in liquefiable soils: 3D parallel finite element modeling. Structures, 74. Elsevier; 2025, 108578. https://doi.org/10.1016/j.istruc.2025.108578.
[20] Forcellini D. A 3-DOF system for preliminary assessments of the interaction between base isolation (BI) technique and soil–structure interaction (SSI) effects for low-rise buildings. Structures, 59. Elsevier; 2024, 105803. https://doi.org/10.1016/j.istruc.2023.105803.
[21] Forcellini D. Key parameters to model the mutual effects between base isolation (BI) and Soil–Structure interaction (SSI). Appl Sci 2024;14(24):2076–3417.
[22] Fiamingo A, Massimino MR. Geotechnical Analyses for the Preservation of Historical Churches: A Case-History in Eastern Sicily (Italy). In: Perkowski Z, Beben D, Zembaty Z, Massimino MR, Oliveira MJ, editors. Environmental Challenges in Civil Engineering III. ECCE 2024. Lecture Notes in Civil Engineering. 615. Cham.: Springer; 2025. p. 23–38. https://doi.org/10.1007/978-3-031-73776-3_2.
[23] Mina D, Forcellini D. Soil–structure interaction assessment of the 23 November 1980 Irpinia-Basilicata earthquake. Geosciences 2020;10(4):152. https://doi.org/10.3390/geosciences10040152.
[24] Massimino MR, Abate G, Fiamingo A, Pitilakis D. Seismic Risk and Environmentally Friendly Solutions: The Geotechnical Point of View. In: Zembaty Z, Perkowski Z, Beben D, Massimino MR, Lavan O, editors. Environmental Challenges in Civil Engineering II. ECCE 2022. Lecture Notes in Civil Engineering. 322. Cham: Springer; 2023. https://doi.org/10.1007/978-3-031-26879-3_1.
[25] Abate G, Fiamingo A, Massimino MR. The Role of DSSI on the Seismic Risk Assessment of a Building. In: Zembaty Z, Perkowski Z, Beben D, Massimino MR, Lavan O, editors. Environmental Challenges in Civil Engineering II. ECCE 2022. Lecture Notes in Civil Engineering. 322. Cham: Springer; 2023. https://doi.org/10.1007/978-3-031-26879-3_4.
[26] Farhad AAA, Aydın E. Viscous damper optimization in Low-Rise adjacent buildings exposed to earthquakes by considering the Soil-Structure interaction. Buildings 2025;15(2):260. https://doi.org/10.3390/buildings15020260.
[27] Kalfas KN, Amirabad NG, Forcellini D. The role of shear modulus on the mechanical behavior of elastomeric bearings when subjected to combined axial and shear loads. Eng Struct 2021;248:113248. https://doi.org/10.1016/j.engstruct.2021.113248.
[28] Gutierrez Soto M, Adeli H. Tuned mass dampers. Arch Comput Methods Eng 2013;20:419–31.
[29] Rana R, Soong TT. Parametric study and simplified design of tuned mass dampers. Eng Struct 1998;20(3):193–204.
[30] Sadek F, Mohraz B, Taylor AW, Chung RM. A method of estimating the parameters of tuned mass dampers for seismic applications. Earthq Eng Struct Dyn 1997;26(6):617–35.
[31] Konar T, Ghosh AD. Tuned mass damper inerter for seismic control of multi-story buildings: ten years since inception (May). Structures, 63. Elsevier; 2024, 106459 (May).
[32] Marrazzo PR, Montuori R, Nastri E, Benzoni G. Advanced seismic retrofitting with high-mass-ratio tuned mass dampers. Soil Dyn Earthq Eng 2024;179:108544.
[33] Araz o. Effect of basic parameters defining principal soil-structure interaction on seismic control of structures equipped with optimum tuned mass damper. Soil Dyn Earthq Eng 2025;189:109085. https://doi.org/10.1016/j.soildyn.2024.109085.
[34] Fatollahpour A, Tafakori E, Arjmandi SAA. The effects of structure-soil-structure interaction on seismic response of high-rise buildings equipped with optimized tuned mass damper. Structures, 50. Elsevier; 2023. p. 998–1010. https://doi.org/10.1016/j.istruc.2023.01.132.
[35] Computers and Structures, Inc. SAP2000 (Version 23.1.1) [Computer software]. Berkeley, California: Computers and Structures, Inc; 2021.
[36] Carvalho G, Bento R, Bhatt C. Nonlinear static and dynamic analyses of reinforced concrete buildings—Comparison of different modelling approaches. Earthq. Struct. 2013;4:451–70. https://doi.org/10.12989/eas.2013.4.5.451.
[37] Newmark NM. A method of computation for structural dynamics. J Eng Mech Div 1959;85(3):67–94.
[38] Pais A, Kausel E. Approximate formulas for dynamic stiff nesses of rigid foundations. Soil Dyn Earthq Eng 1998;7(4):213–27. https://doi.org/10.1016/S0267-7261(88)80005-8.
[39] Zheng G, Zhang W, Zhou H, Forcellini D, Zhao J, Zhang T. 3D numerical modeling of the inertial and kinematic interactions of inclined pile groups in liquefiable soils. Int J Geomech 2024;24(8):04024161. https://doi.org/10.1061/IJGNAI.GMENG-9705.
[40] Asgari A, Bagheri M, Hadizadeh M. Advanced seismic analysis of soil-foundation-structure interaction for shallow and pile foundations in saturated and dry deposits: insights from 3D parallel finite element modeling. Structures, 69. Elsevier; 2024, 107503. https://doi.org/10.1016/j.istruc.2024.107503.
[41] Asgari A, Sorkhi SFA. Wind turbine performance under multi-hazard loads: wave, wind, and earthquake effects on liquefiable soil. Results Eng 2025;26:104647.
[42] NIST G. Soil-structure interaction for building structures. Natl Earthq Hazards Reduct Program (NEHRP) 2012;12.
[43] Tsang HH, Pitilakis K. Mechanism of geotechnical seismic isolation system: analytical modeling. Soil Dyn Earthq Eng 2019;122(Jul):171–84. https://doi.org/10.1016/j.soildyn.2019.03.037.
[44] Oz I. Seismic pounding effects of typical midrise reinforced concrete structures subjected to Soil–Structure interaction effects. J Struct Eng 2025;151(2):05024005.
[45] Oz Ibrahim. Resilience of hospital structures under seismic loads: a case study informed by the 2023 Maraş earthquake (April). Structures, 74. Elsevier; 2025, 108642 (April).
[46] Oz I, Senel SM, Palanci M, Kalkan A. Effect of soil-structure interaction on the seismic response of existing low and mid-rise RC buildings. Appl. Sci. 2020;10:8357. https://doi.org/10.3390/app10238357.
[47] TBEC. Turkish Building Earthquake Code; Ministry of Environment and Urban Planning: Ankara, Turkey, 2018. (In Turkish).
[48] NEHRP. NEHRP recommended provisions for seismic regulations for new buildings and other structures (National Earthquake Hazards Reduction Program)). Washington, DC: FEMA; 2001.
[49] ASCE. Minimum design loads for buildings and other structures. ASCE/SEI 7-10. Reston, VA: ASCE; 2010.
[50] Elwardany H, Seleemah A, Jankowski R, El-Khoriby S. Influence of soil–structure interaction on seismic pounding between steel frame buildings considering the effect of infill panels. Bull Earthq Eng 2019;17(11):6165–202. https://doi.org/10.1007/s10518-019-00713-1.
[51] Connor JJ. Introduction to structural motion control. Upper Saddle River: Prentice Hall/Pearson Education; 2003.
[52] PEER. Pacific Earthquake Engineering Research Center. Strong ground motion database. Accessed November 2024. ⟨https://ngawest2.berkeley.edu/⟩.
[53] Bosco M, Fiamingo A, Massimino MR, Rossi PP. An assessment of the seismic performance of EC8-Compliant CBFs taking into account the role of soil: a case study. Buildings 2024;14(7):2161. https://doi.org/10.3390/buildings14072161.
[54] Stefanidou SP, Sextos AG, Kotsoglou AN, Lesgidis N, Kappos AJ. Soil-structure interaction effects in analysis of seismic fragility of bridges using an intensity-based ground motion selection procedure. Eng Struct 2017;151:366–80. https://doi.org/10.1016/j.engstruct.2017.08.033.
[55] Khosravikia F, Mahsuli M, Ghannad MA. The effect of soil–structure interaction on the seismic risk to buildings. Bull Earthq Eng 2018;16:3653–73. https://doi.org/10.1007/s10518-018-0314-z.
[56] AFAD). (2023). Türkiye Deprem Tehlike Haritaları (TDTH) [Interactive web application]. Available from: ⟨https://tdth.afad.gov.tr/TDTH/main.xhtml⟩.
[57] Forcellini D. Analytical fragility curves of shallow-founded structures subjected to Soil-Structure interaction (SSI) effects. Soil Dyn Earthq Eng 2021;141:106487. https://doi.org/10.1016/j.soildyn.2020.106487.
[58] Forcellini D, Alzabeebee S. Seismic fragility assessment of geotechnical seismic isolation (GSI) for bridge configuration. Bull Earthq Eng 2023;21(8):3969–90. https://doi.org/10.1007/s10518-022-01356-5.